Supporting Information

Ru doping and interface engineering synergistically boosting the electrocatalytic performance of WP/WP_2 nanosheet array for efficient hydrogen evolution reaction

Zhichang Hu[a], Zhizhong Xiao[a], Wei Wei[a], Jian Yang[a], Xiaoyu Huang[a], Qingcheng Lu[a], Sundaram Chandrasekaran[a], Huidan Lu[*a], and Yongping Liu[*a]

[a]*Guangxi Key Laboratory of Electrochemical and Magneto-chemical Functional Materials, College of Chemistry and Bioengineering, Guilin University of Technology, Guilin 541004, P. R. China.*

*Corresponding authors.

E-mail address: lhuidangl@163.com (Lu H); liuyp624@163.com (Liu Y)

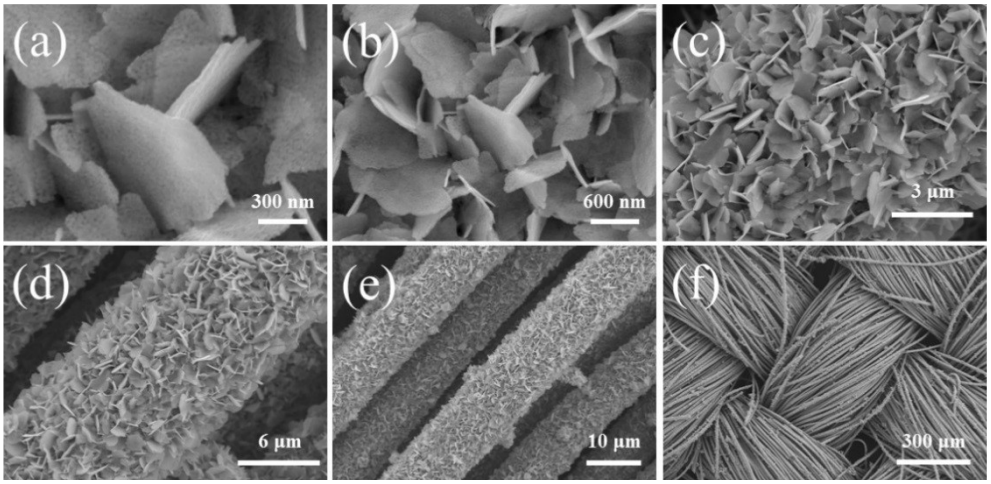

Fig. S1. SEM images of Ru-WO_3 NS/CC.

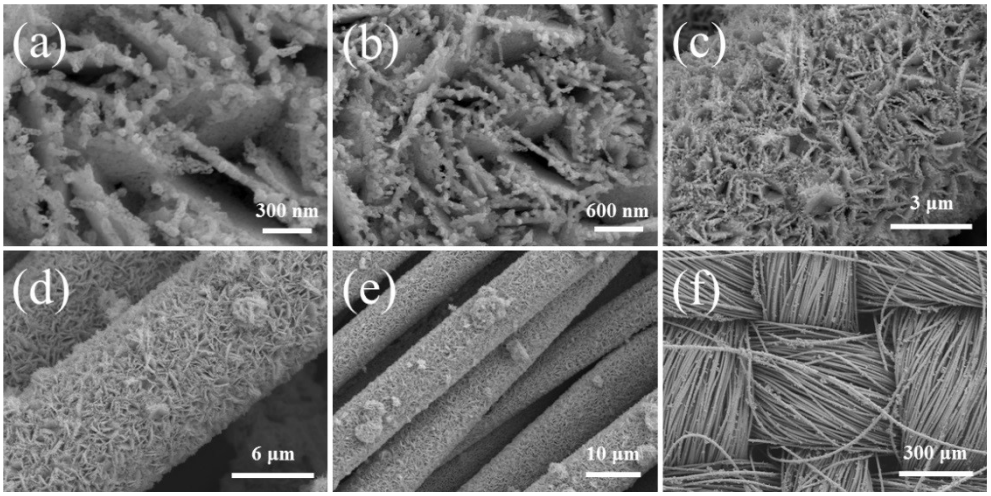

Fig. S2. SEM images of Ru-WP/WP_2 NH/CC.

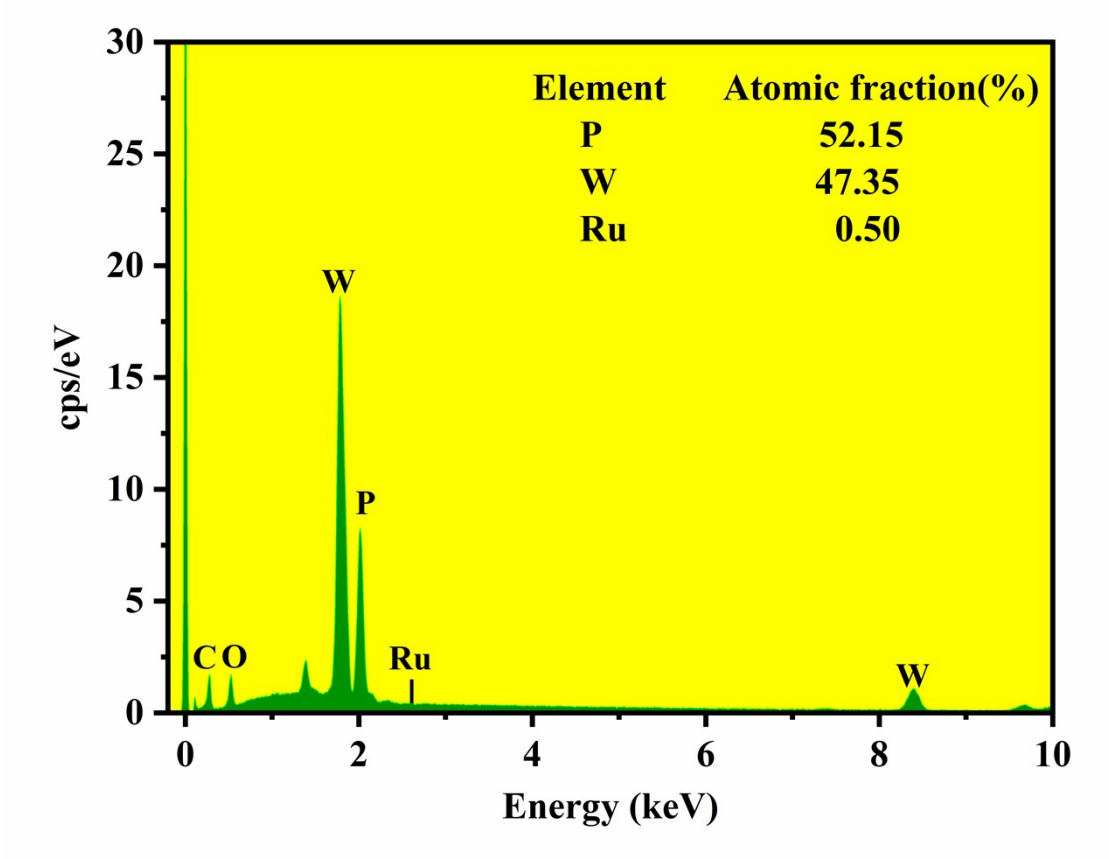

Fig. S3. EDS result of Ru-WP/WP_2 NH/CC.

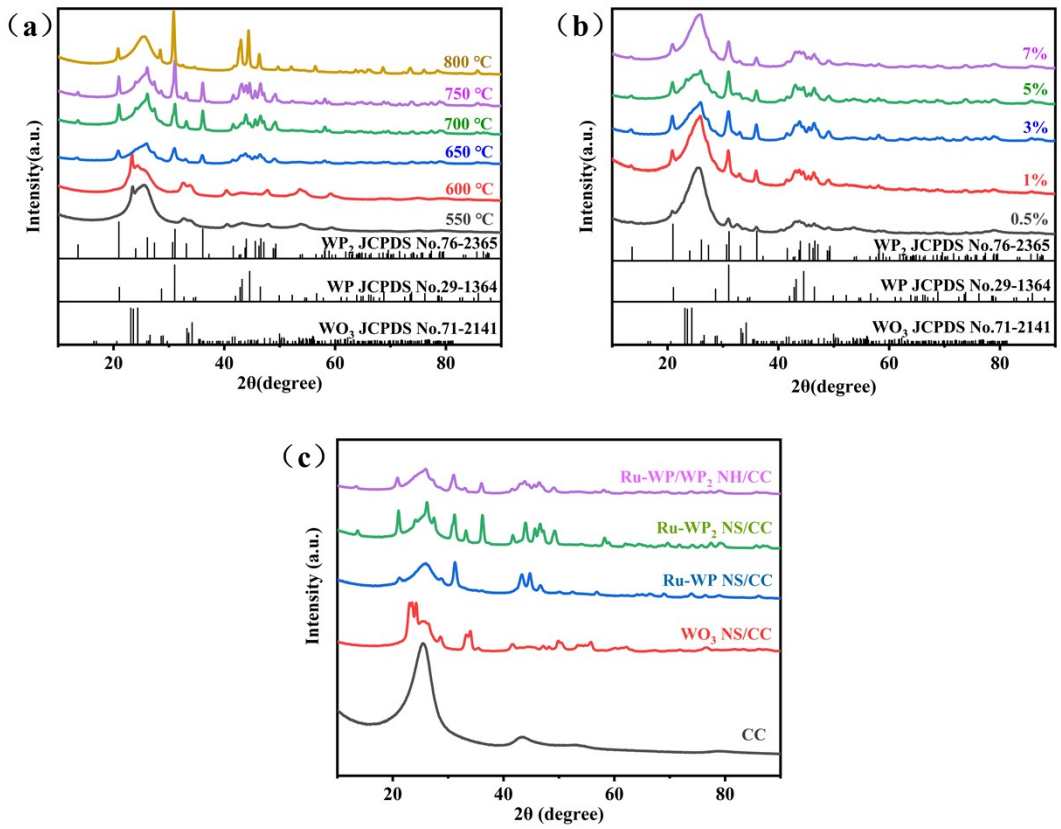

Fig. S4. XRD pattern of Ru catalyst. (a) Temperature optimization gradient. (b) Different Ru doping. (c) Comparison with bare carbon cloth.

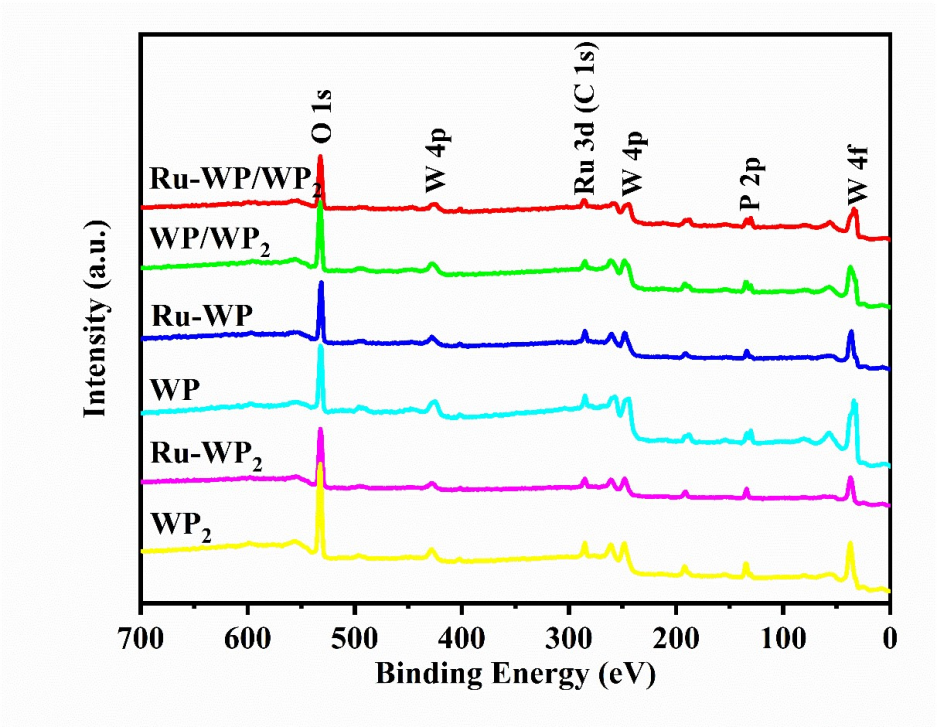

Fig. S5. XPS spectra of Survey spectrum.

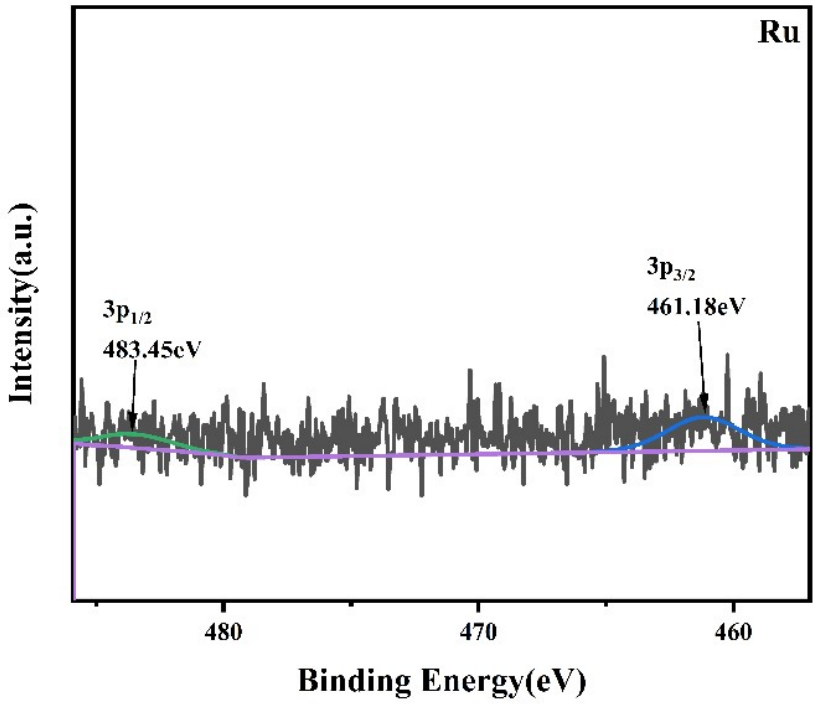

Fig. S6. XPS spectra of Ru 3p

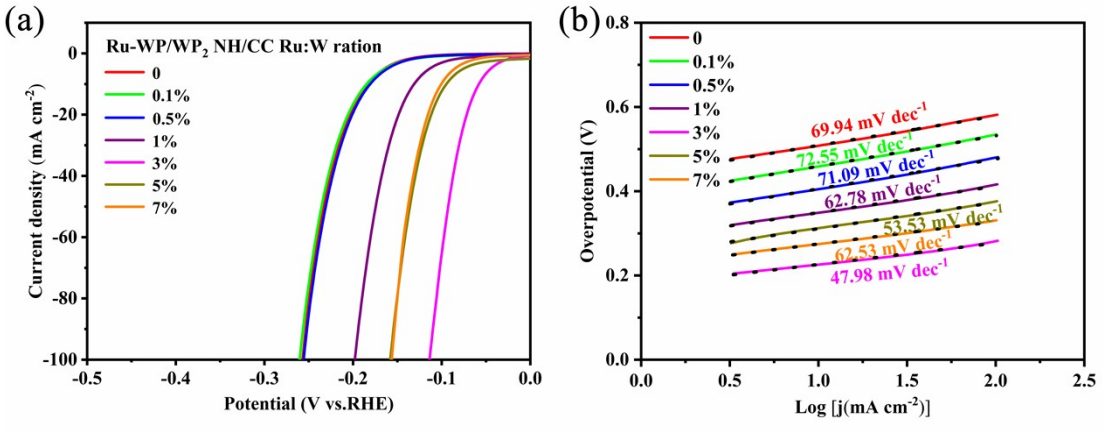

Fig. S7. The Ru: W ratio added to the precursor sample was optimized. (a) Linear sweep voltammetry of the catalyst at a scanning rate of 5 mV s^{-1}, and (b) Tafel slope.

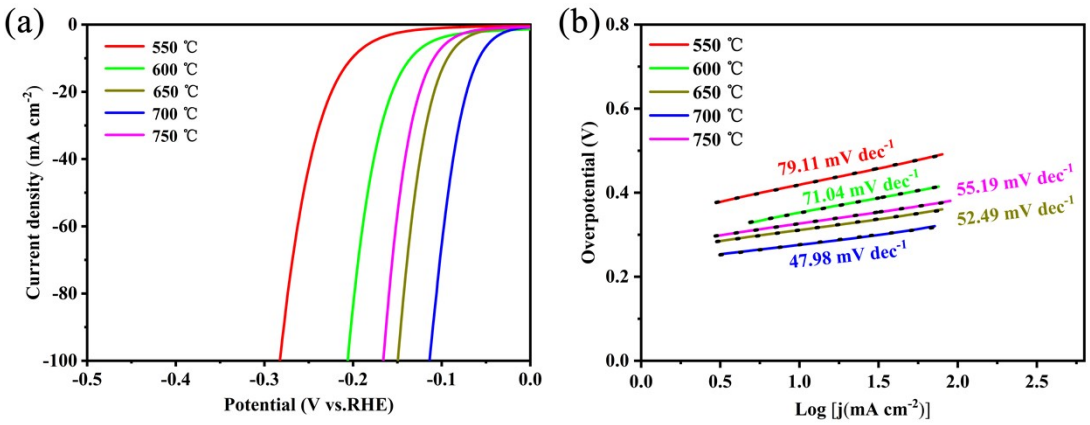

Fig. S8. Temperature gradient optimization of catalyst. (a) Linear sweep voltammetry of the catalyst at a scanning rate of 5 mV s^{-1} and (b) Tafel slope.

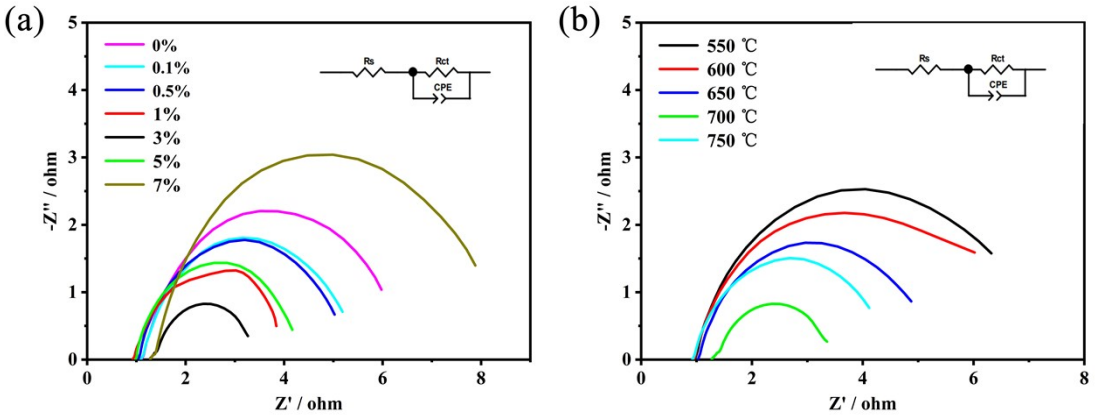

Fig. S9. Nyquist curves for (a) different Ru doping concentrations, and (b) different phosphating temperatures.

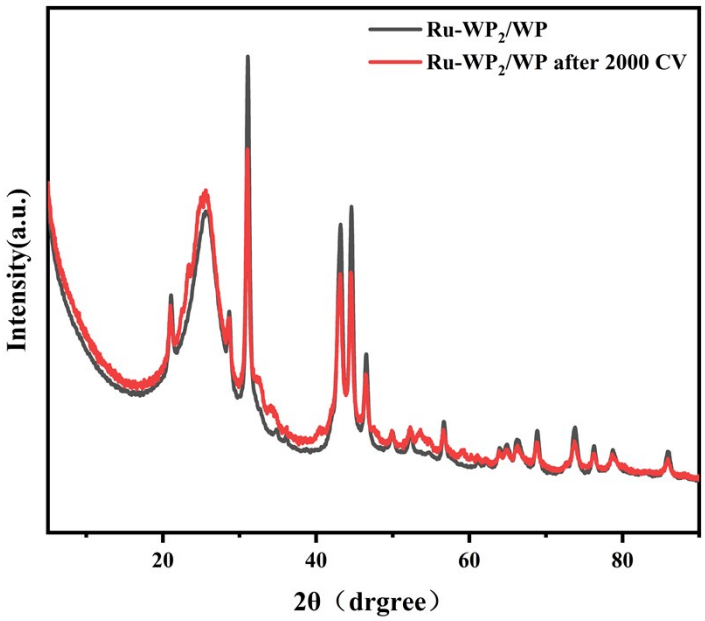

Fig. S10. XRD comparison of Ru-WP_2/WP before and after 2000 cycles CV

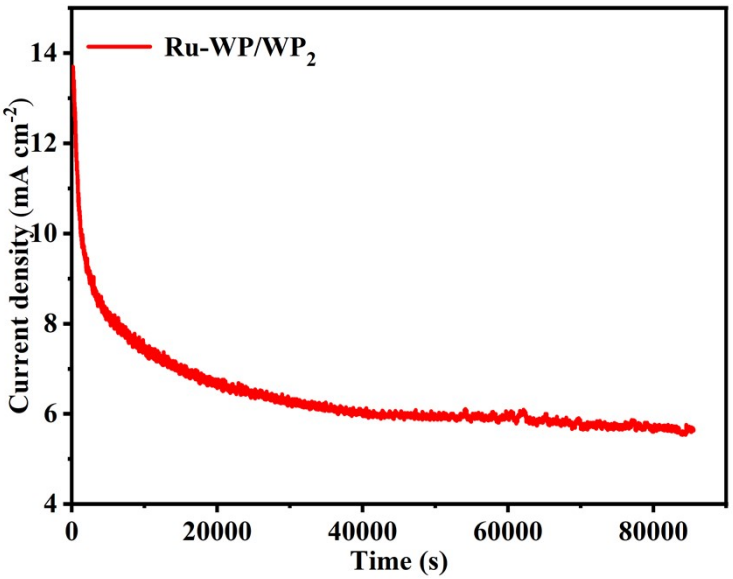

Fig. S11. The stability curve of 3% Ru-WP_2/WP tested at 10 mA cm^{-2}.

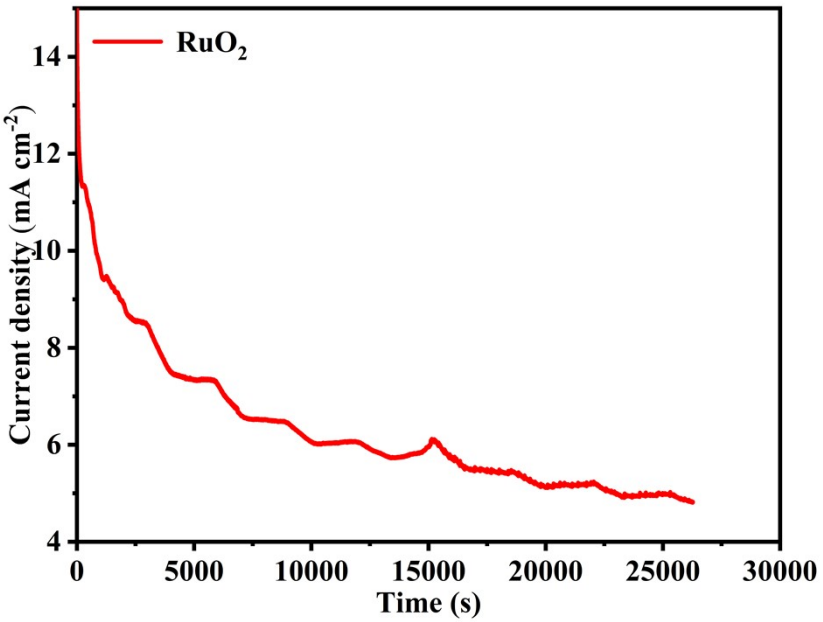

Fig. S12. The stability curve of RuO_2 tested at 10 mA cm^{-2}.

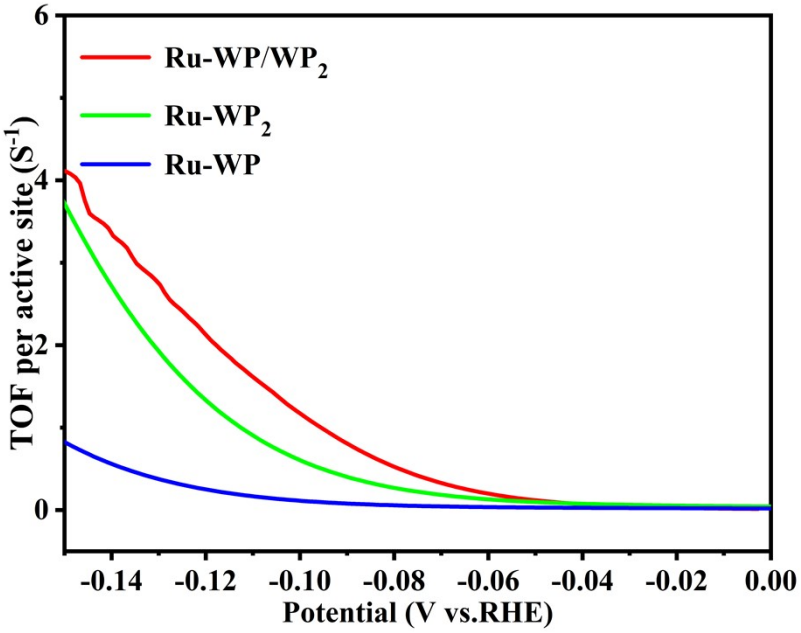

Fig. S13. TOF curves of Ru-WP_2/WP, Ru-WP_2 and Ru-WP.

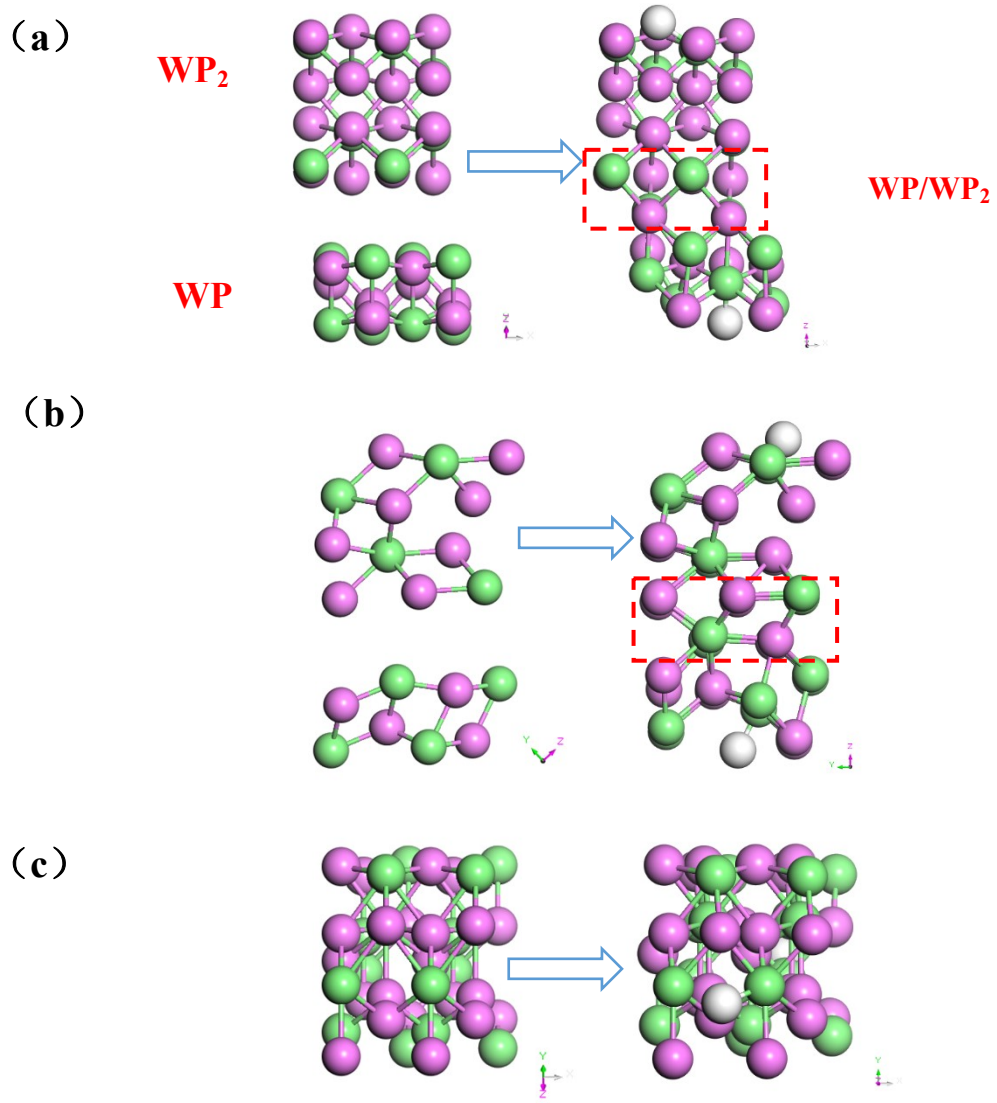

Fig. S14. WP/WP_2 optimization front and rear models, the left is optimized before the left is optimized. (a) Front view, (b) Side view, and (c) Top view. White, Green and Pink balls represent H, W and P atoms, respectively. The heterojunction interface and interface atoms were highlighted in (a) and (b).

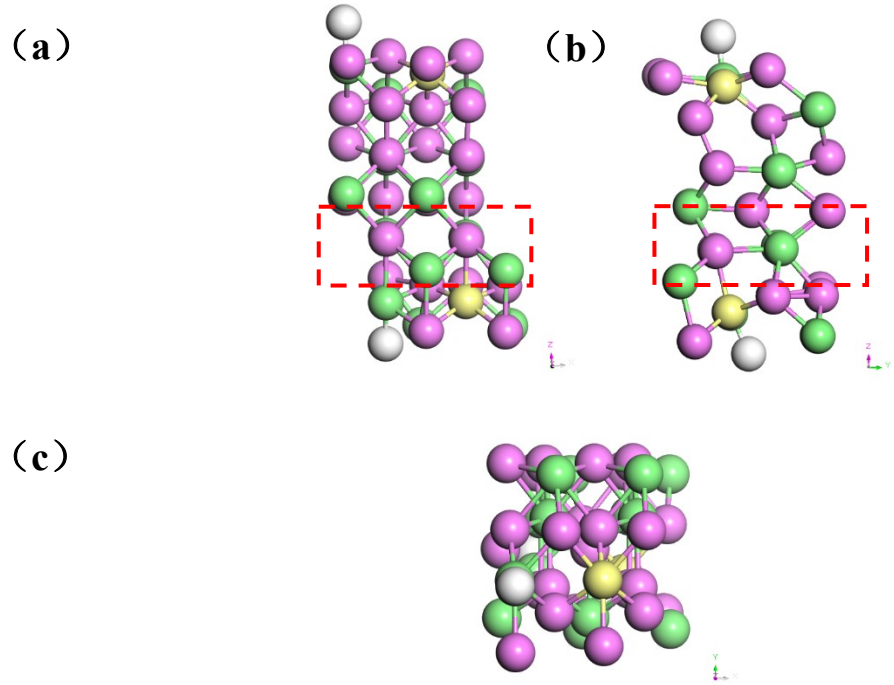

Fig. S15. Ru-WP/WP_2 model and after structural optimization. (a) Front view, (b)Side view, and (c) Top view. Yellow, White, Green and Pink balls represents Ru, H, W and P atoms, respectively. The heterojunction interface and interface atoms were highlighted in (a) and (b).

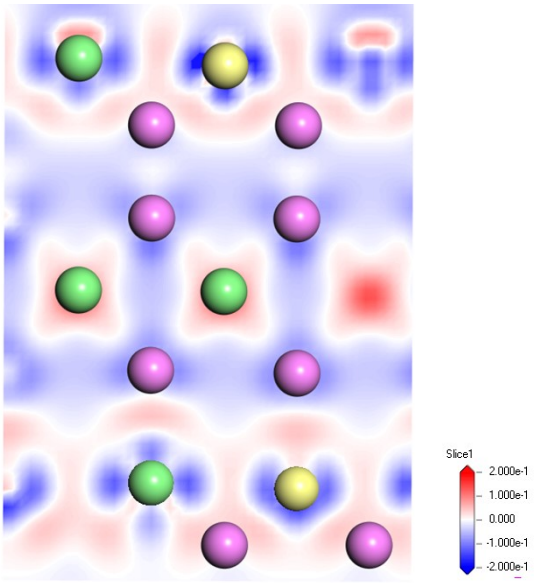

Fig. S16. Charge density difference diagram of Ru-WP/WP_2.

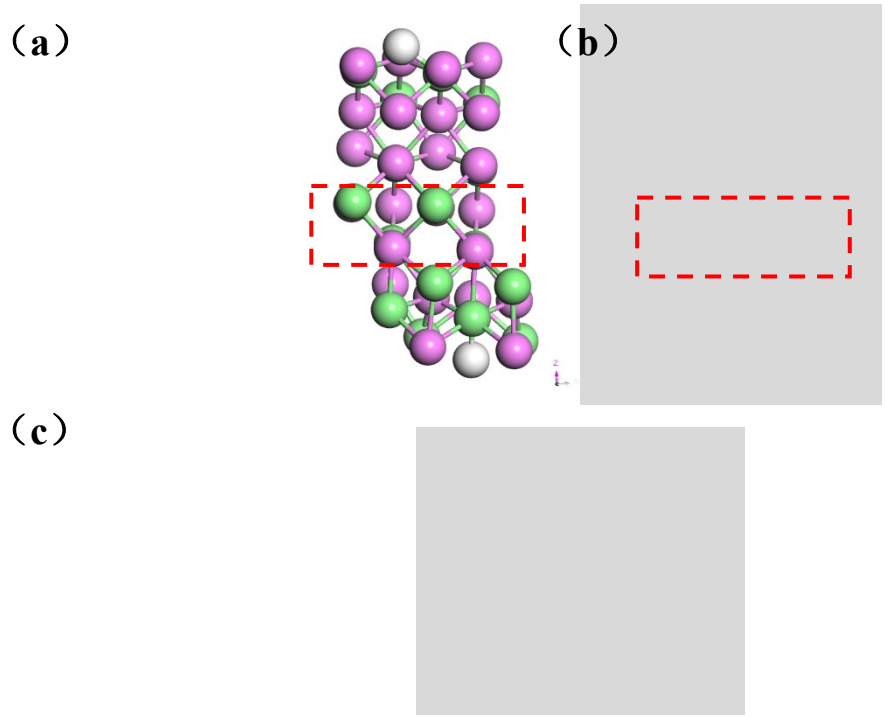

Fig. S17. WP/WP_2 model at after structural optimization. (a) Front view, (b) Side view, (c) Top view. White, Green and Pink balls represent H, W, and P atoms, respectively. The heterojunction interface and interface atoms were highlighted in (a) and (b).

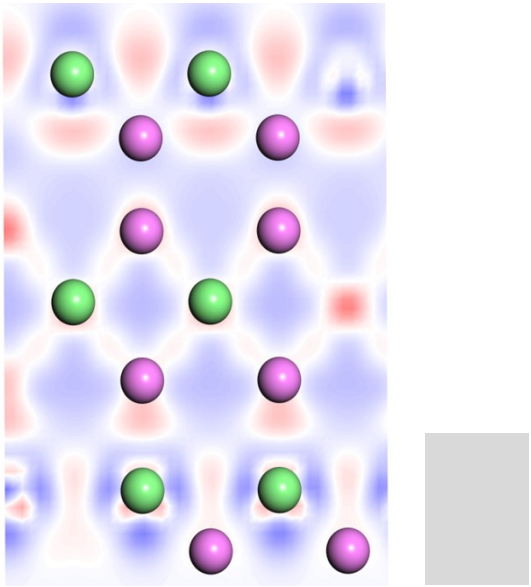

Fig. S18. Charge density difference diagram of WP/WP_2.

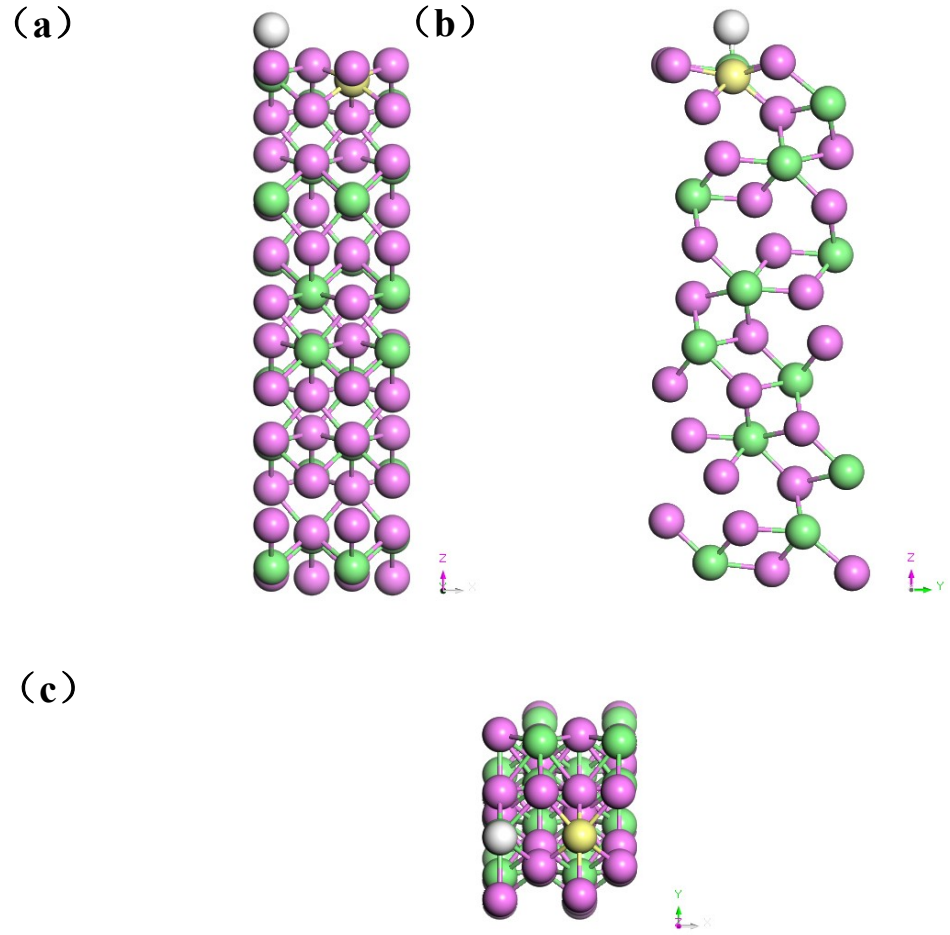

Fig. S19. Optimized atomic model for Ru-WP_2 (a) Front view, (b) Side view, and (c) Top view. Yellow, White, Green, and Pink balls represent Ru, H, W and P atoms, respectively.

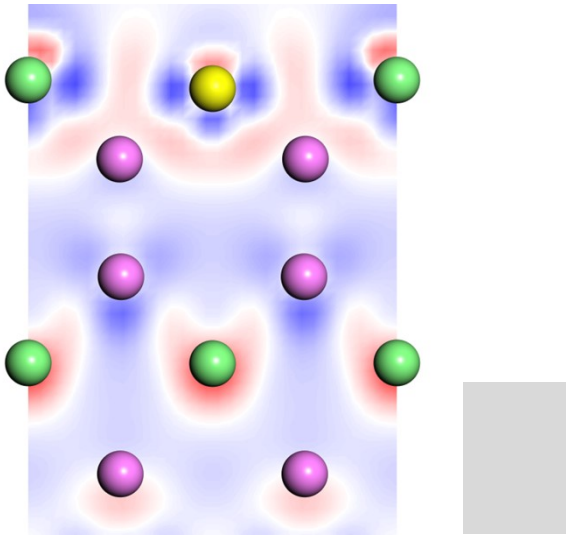

Fig. S20. Charge density difference diagram of Ru-WP_2.

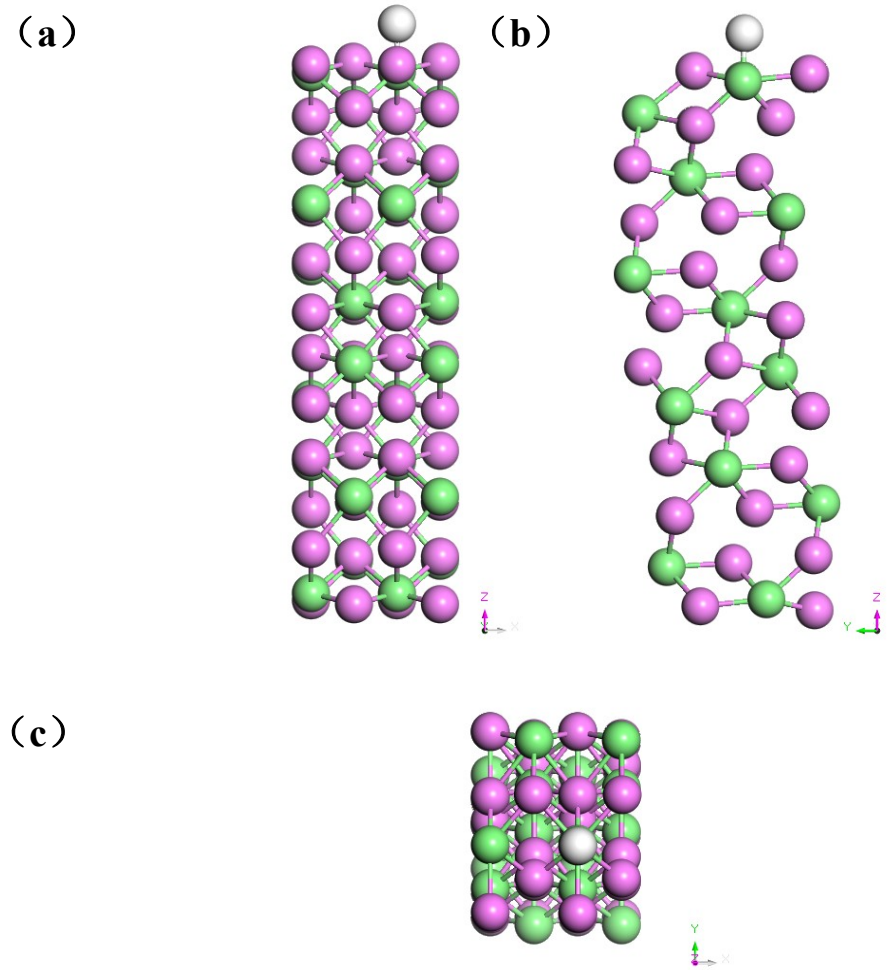

Fig. S21. WP_2 model and after structural optimization. (a) Front view, (b) Side view, and (c) Top view. White, Green, and Pink balls represent H, W, and P atoms, respectively.

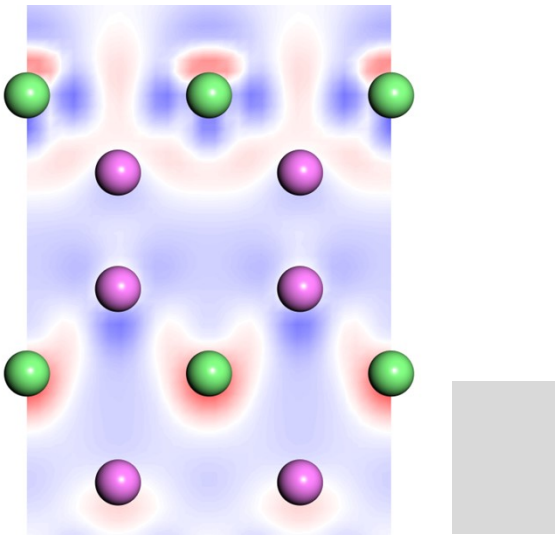

Fig. S22. Charge density difference diagram of WP_2.

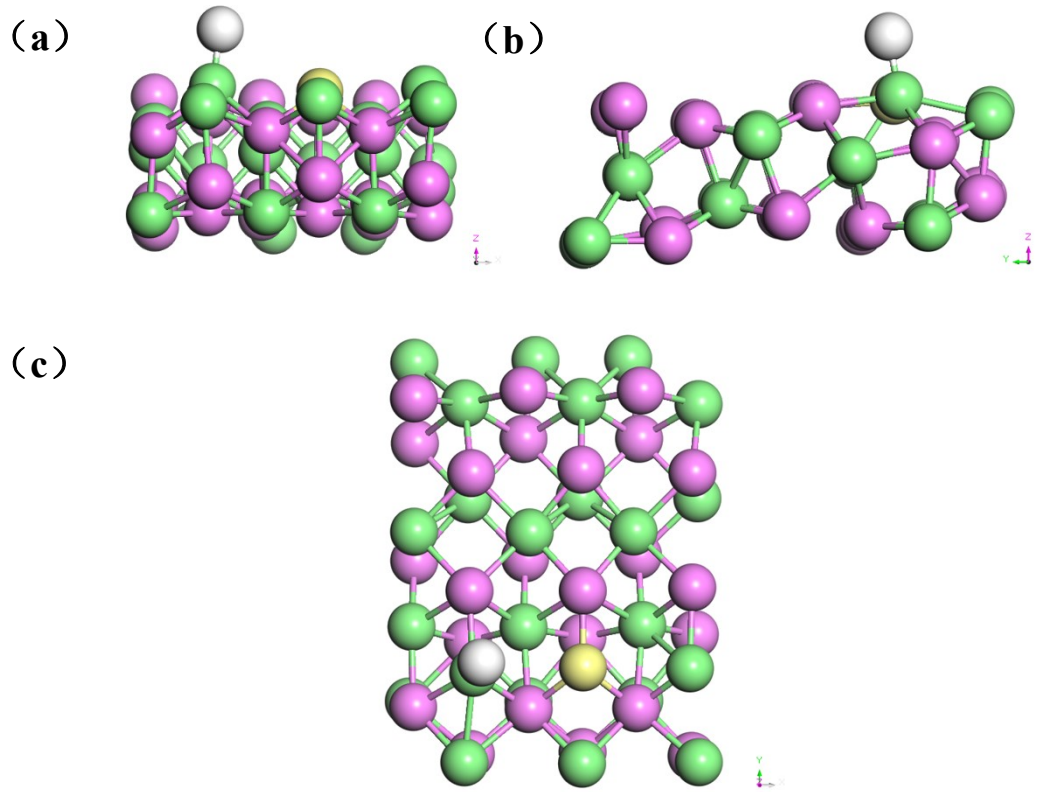

Fig. S23. Ru-WP model and after structural optimization. (a) Front view, (b) Side view, and (c) Top view. Yellow, White, Green, and Pink balls represent Ru, H, W, and P atoms, respectively.

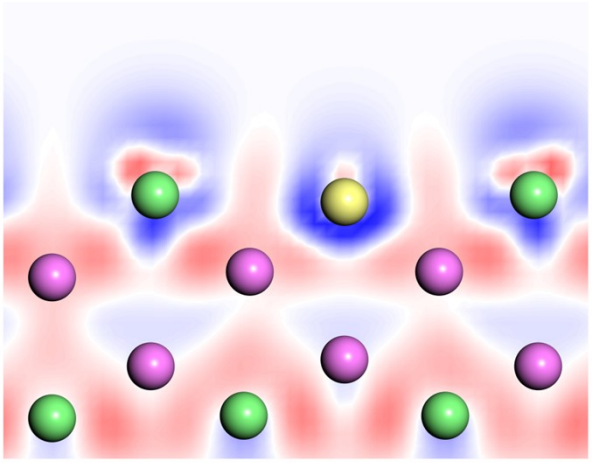

Fig. S24. Charge density difference diagram of Ru-WP.

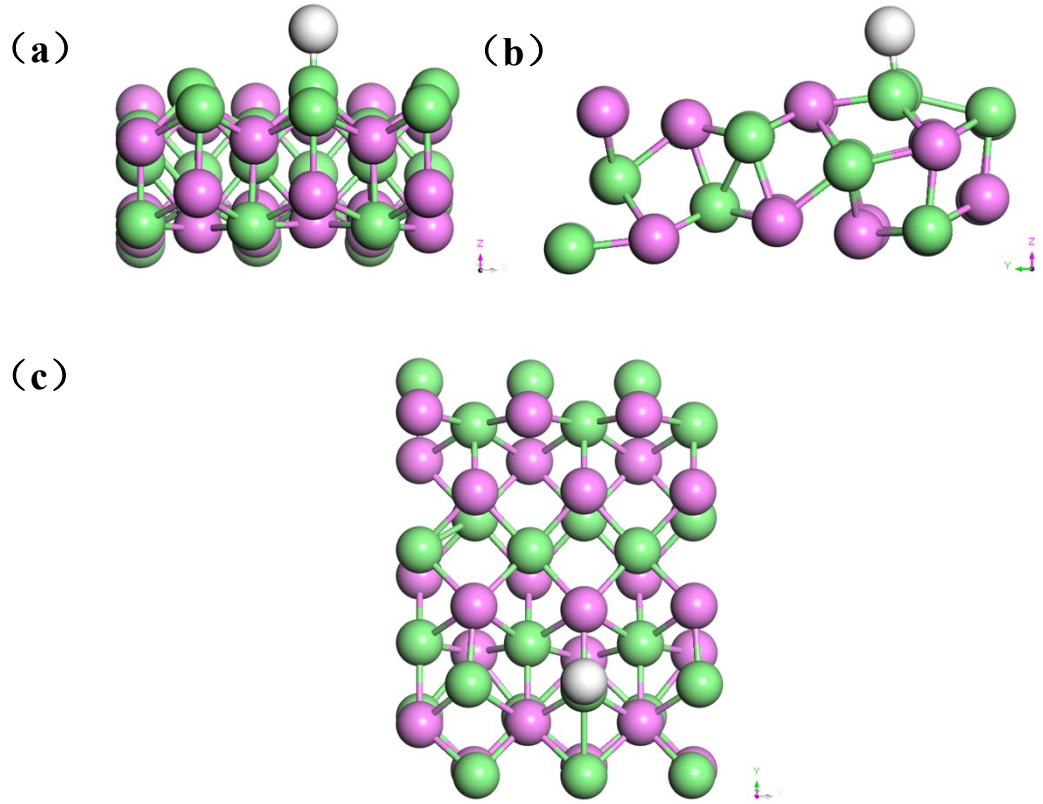

Fig. S25. WP model and after structural optimization. (a) Front view, (b) Side view, (c) Top view. White is an H atom, green is W atom and pink is P atom.

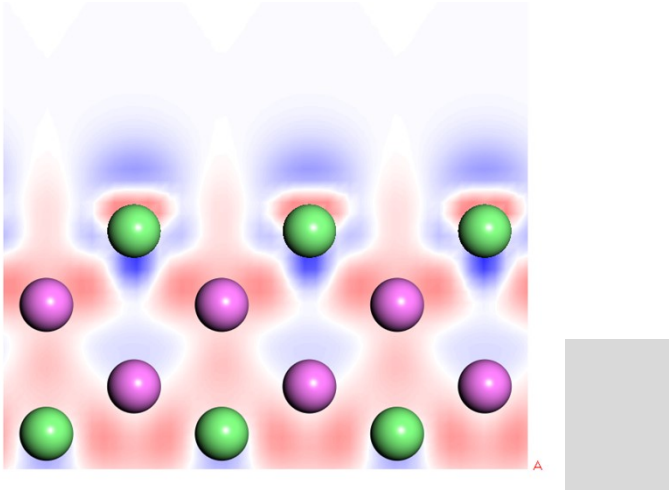

Fig. S26. Charge density difference diagram of WP.

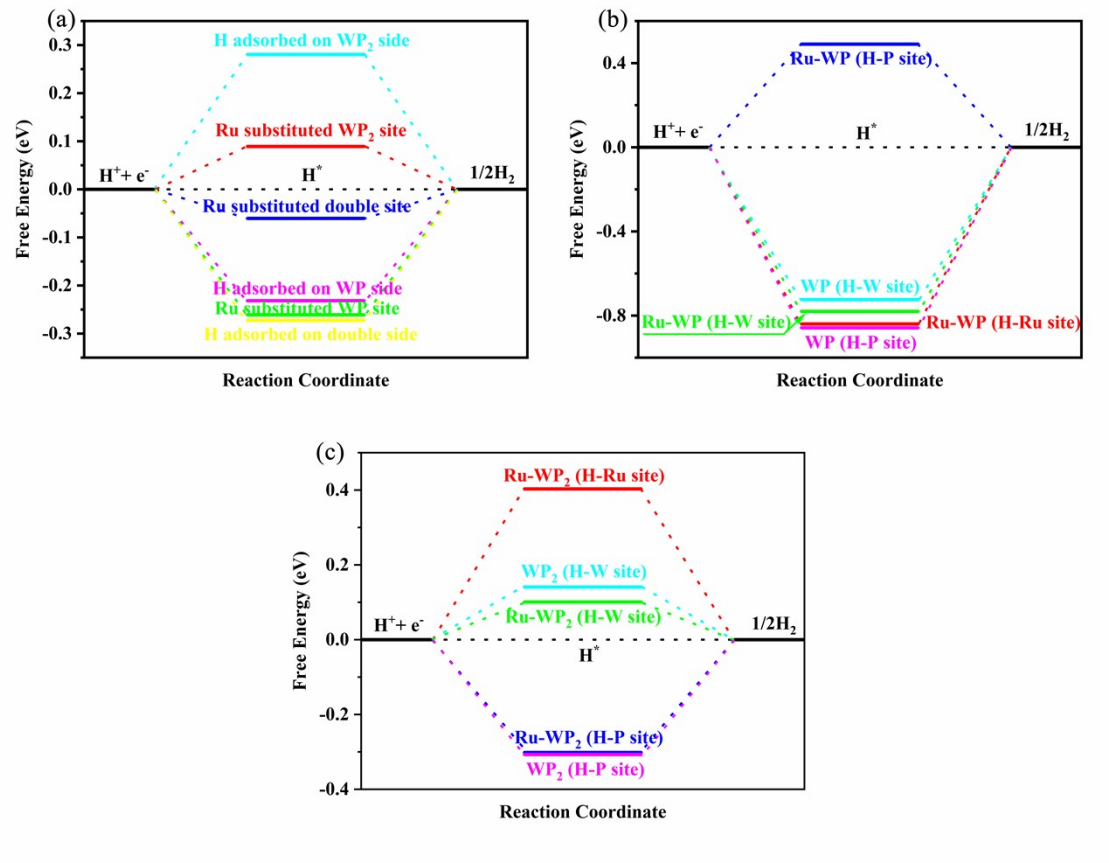

Fig. S27. Gibbs free energy volcano diagram of hydrogen adsorption point of catalyst.

(a) Ru-WP/WP_2 NH/CC. (b) Ru-WP NS/CC, and (c) Ru- WP_2 NS/CC.

Table S1. Acidic HER performance of catalysts prepared with different Ru: W ratio.

Electrocatalyst[a]	Overpotential (mV *vs.* RHE)	Tafel slope (mV dec^{-1})	R_{ct} (Ω)	The atomic ratio of Ru to W[b]
0	183.8	69.64	5.26	0
0.1%	184.7	72.55	4.27	0.22%
0.5%	180.7	71.09	4.17	0.61%
1%	131.1	62.78	3.04	2.6%
3%	58.0	47.98	2.20	4.2%
5%	94.7	62.53	3.19	5.61%
7%	100.4	53.53	7.10	6.1%

[a]The Ru: W ratio% joined when the catalyst was prepared.

[b]The results of ICP data analysis

Table S2. Acidic HER activities of Ru-WP/WP_2 NH/CC catalysts prepared at different phosphating temperatures. (Temperature effect on optimized Ru-WP/WP_2 NH/CC)

Electrocatalyst[a]	Overpotential (mV *vs.* RHE)	Tafel slope(mV dec^{-1})	R_{ct} (Ω)
550	201.2	71.11	6.21
600	134.9	71.04	5.52
650	94.1	52.49	4.19
700	58.0	47.98	2.20
750	108.8	55.19	3.45

[a] The catalysts of prepared at different phosphating temperatures.

Table S3. Summarized HER performance of some previously reported catalysts with present work.

Electrocatalyst	Overpotential (mV *vs.* RHE)	Tafel slope (mV dec^{-1})	Reference
Ru-WP/WP_2	58	47.98	This work
ES-WC/W_2C	75	59	[1]
NiP_2/CoP_2	71	48.5	[2]
Mo_2C@MoS_2	67	67	[3]
CoP_3/CoMoP/NF	125	61.1	[4]
MoS_2-MoP	102	58	[5]
CoP/Co-MOF	52	49	[6]
Co-Mo_5N_6	19	29	[7]
CoP/NiCoP	133	88	[8]
Se-MnS/NiS	56	55	[9]
Ru-NiCoP/NF	44	45.4	[10]
Ru-CuO/MoS_2	198	113	[11]
Ru-$Zn_3V_3O_8$	70	50.6	[12]
Ru-FeCoP	45	32.1	[13]
Ru-VN	134	35	[14]
Ru-NMCNs-T	28	35.2	[15]
Pd–Ru@NG	42	73	[16]
Ru@B–$Ti_3C_2T_x$	62.9	100	[17]

Ru/CoO	55	72	[18]
NiFe-P	44	80	[19]
WP_2 NW/NF	130	94	[20]
Ni-WP_2 NS/CC	110	65	[21]
CoWP-CA/KB	111	58	[22]
WP-Mesop	104	58	[23]
Co/WP_2 NWs	72	52	[24]
W-Ni_2P NS/CC	71	67.4	[25]
P-WP_2 NSs/GP	155	66	[26]
C-WP/W	109	79.8	[27]

Table S4. Gibbs free energy of adsorbed hydrogen at each point of the catalyst.

Electrocatalyst	Adsorption site of H	ΔG_{H^*} (eV)
Pt	Pt	-0.09
Ru-WP	Ru	-0.84
	W	-0.71
	P	0.49
WP	W	-0.72
	P	-0.86
Ru-WP_2	Ru	0.40
	W	-0.10
	P	-0.3
WP_2	Ru	0.14
	W	-0.31

Table S5. Gibbs free energy of adsorbed hydrogen with different Ru substitution sites in Ru-WP/WP_2 heterojunction. When Ru is doped, H is adsorbed on the W atom next to Ru.

Electrocatalyst	Ru Substitution Sites		ΔG_{H^*} (eV)
Ru-WP/WP_2	Ru substituted WP_2 side	H adsorbed on WP_2 side	0.089
		H adsorbed on WP side	-0.241
	Ru substituted WP side	H adsorbed on WP_2 side	0.175
		H adsorbed on WP side	-0.261
	Both WP and WP_2 are replaced by Ru	H adsorbed on WP_2 side	0.119
		H adsorbed on WP side	-0.235
		H adsorption on both sides of WP and WP_2.	-0.06
WP/WP_2	H adsorbed on WP_2 side		0.281
	H adsorbed on WP side		-0.232
	H adsorption on both sides of WP and WP_2.		-0.272

References

[1] Z. Chen, W. Gong, S. Cong, Z. Wang, G. Song, T. Pan, X. Tang, J. Chen, W. Lu, Z. Zhao, Nano Energy 68 (2020) 104335.

[2] M. Patel, M. Ali, J. Ahmad, M. Dar, K. Majid, S. Lone, D. Puthusseri, M. Wahid, Mater. Lett. 278 (2020) 128456.

[3] S. Yang, Y. Wang, H. Zhang, Y. Zhang, L. Liu, L. Fang, X. Yang, X. Gu, Y. Wang, J. Catal. 371 (2019) 20-26.

[4] D. Jiang, Y. Xu, R. Yang, D. Li, S. Meng, M. Chen, ACS Sustain. Chem. Eng. 7 (2019) 9309-9317.

[5] Z. Wu, J. Wang, K. Xia, W. Lei, X. Liu, D. Wang, J. Mater. Chem. A 6 (2018) 616-622.

[6] Q. Li, Y. Zhou, C. Chen, Q. Liu, J. Huo, H. Yi, J. Electroanal. Chem. 895 (2021).

[7] F. Lin, Z. Dong, Y. Yao, L. Yang, F. Fang, L. Jiao, Adv. Energy Mater. 10 (2020) 2002176.

[8] Y. Lin, K. Sun, S. Liu, X. Chen, Y. Cheng, W. C. Cheong, Z. Chen, L. Zheng, J. Zhang, X. Li, Y. Pan, C. Chen, Adv. Energy Mater. 9 (2019) 1901213.

[9] J. Zhu, M. Sun, S. Liu, X. Liu, K. Hu, L. Wang, J. Mater. Chem. A 7 (2019) 26975-26983.

[10] D. Chen, R. Lu, Z. Pu, J. Zhu, H.-W. Li, F. Liu, S. Hu, X. Luo, J. Wu, Y. Zhao, S. Mu, Appl. Catal. B 279 (2020) 119396.

[11] A. Maiti, S. K. Srivastava, ACS Appl. Nano Mater. 4 (2021) 7675-7685.

[12] X. Zhou, X. Tang, H. Xu, T. Jiang, K. Hu, H. J. Qiu, X. Lin, Nanoscale 13 (2021) 17457-17464.

[13] H. Liu, X. Li, L. Ge, C. Peng, L. Zhu, W. Zou, J. Chen, Q. Wu, Y. Zhang, H. Huang, J. Wang, Z. Cheng, Z. Fu, Y. Lu, Catal. Sci. Technol. 10 (2020) 8314-8324.

[14] W. Wang, Y. Shao, Z. Wang, Z. Yang, Z. Zhen, Z. Zhang, C. Mao, X. Guo, G. Li, ChemElectroChem 7 (2020) 1201-1206.

[15] J. Peng, Y. Chen, K. Wang, Z. Tang, S. Chen, Int. J. Hydrogen Energy 45 (2020) 18840-18849.

[16] B. K. Barman, B. Sarkar, K. K. Nanda, Chem. Commun. 55 (2019) 13928-13931.

[17] M. Bat-Erdene, M. Batmunkh, B. Sainbileg, M. Hayashi, A. S. R. Bati, J. Qin, H. Zhao, Y. L. Zhong, J. G. Shapter, Small 17 (2021) e2102218.

[18] J.-X. Guo, D.-Y. Yan, K.-W. Qiu, C. Mu, D. Jiao, J. Mao, H. Wang, T. Ling, J. Energy Chem. 37 (2019) 143-147.

[19] M. Qu, Y. Jiang, M. Yang, S. Liu, Q. Guo, W. Shen, M. Li, R. He, Appl. Catal. B 263 (2020) 118324.

[20] F. Meng, Y. Yu, D. Sun, L. Li, S. Lin, L. Huang, W. Chu, S. Ma, B. Xu, Appl. Surf. Sci. 546 (2021) 148926.

[21] W. Liu, P. Geng, S. Li, W. Liu, D. Fan, H. Lu, Z. Lu, Y. Liu, J. Energy Chem. 55 (2021) 17-24.

[22] D. Huo, Z. Sun, Y. Liu, Z. Yu, Y. Wang, A. Wang, ACS Sustain. Chem. Eng. 9 (2021) 12311-12322.

[23] F. Li, C. Wang, X. Han, X. Feng, Y. Qu, J. Liu, W. Chen, L. Zhao, X. Song, H. Zhu, H. Chen, M. Zhao, Z. Deng, J. Wu, P. Zhang, L. Gao, ACS Appl. Mater. Interfaces 12 (2020) 22741-22750.

[24] Y. Yang, X. Feng, Z. Liu, X. Zhang, H. Song, C. Pi, B. Gao, P. K Chu, K. Huo, ChemElectroChem 8 (2021) 1658-1664.

[25] S. Li, Y. Liu, Y. Wu, X. Du, J. Guan, L. Wang, M. Zhang, Int. J. Hydrogen Energy 46 (2021) 37152-37161.

[26] M. Pi, W. Guo, T. Wu, X. Wang, D. Zhang, S. Wang, S. Chen, J. Power Sources 364 (2017) 253-257.

[27] L. Wu, Z. Pu, Z. Tu, I. S. Amiinu, S. Liu, P. Wang, S. Mu, Chem. Eng. J. 327 (2017) 705-712.